Magnetotransport properties of Sb₂Te₃ nanoflake

Yi-Chi Huang [a,b], P.C. Lee [a,c], C.H. Chien [a,c], F.Y. Chiu [a],
Y.Y. Chen [a,d], Sergey R. Harutyunyan [a,e,*]

[a] Institute of Physics, Academia Sinica, Nankang, Taipei 115, Taiwan
[b] Department of Physics, National Central University, Chung Li320, Taiwan
[c] Department of Engineering and System Science, National Tsing Hua University, Hsinchu 300, Taiwan
[d] Graduate Institute of Applied Physics, National Chengchi University, Taipei 106, Taiwan
[e] Institute for Physical Research, NASRA, Ashtarak 0203, Armenia

ARTICLE INFO

ABSTRACT

Magnetotransport properties of a single crystal Sb₂Te₃ topological insulator nanoflake with the thickness of 25 nm, synthesized via a vapor phase deposition method, are studied. The mobility and number of carriers are obtained through the Hall resistance measurement data. The magnetoresistance shows pronounced weak antilocalization effect. Temperature dependence of the phase coherence length confirms the 2D nature of the observed weak antilocalization effect. The fluctuations in the magnetoresistance are attributed to the combined contribution of the universal conductance fluctuation and the Shubnikov de Haas oscillations of the 2D electron gas. The Shubnikov de Haas oscillations reveal two well defined frequencies ascribed to states with spin-up and spin-down polarizations. The Rashba parameter and the energy gap between the two spin polarized subbands have been obtained and were equal to $\delta = 0.75 \times 10^{-11}$ eV m and $\Delta E = 2.4$ meV correspondingly.

1. Introduction

Antimony telluride compound (Sb₂Te₃) known as *p*-type thermoelectric material was widely used for thermoelectric energy conversion near room temperature [1]. The compound has a rhombohedral phase of symmetry with space group D_3^5(R-3m) [2]. The multivalley valence band consists of the upper valence band, UVB (light effective mass holes) and the lower valence band, LVB (heavy effective mass holes) [3]. Recently, Sb₂Te₃ has attracted renewed attention because it was predicted and confirmed that the compound is three-dimensional (3D) topological insulator (TI) [4,5]. TI represents a new state of quantum matter, where bulk energy gap coexists with a single spin-polarized Dirac cone (helical) band structure of the metallic gapless surface states. Thus, the material is nominally insulating in the bulk, but it is able to conduct along their surface. The unique surface states having spin-polarized nature with the spin-up and spin-down currents (protected by time-reversal symmetry) originate as the consequence of strong spin-orbit coupling, inherent for this class of materials [6]. TIs are considered as an ideal base for spintronics, quantum computations, and other applications [7,8]. The surface

states have been directly observed by means of angle-resolved photoemission spectroscopy (ARPES) for many 3D TIs, including Sb₂Te₃ [5]. Some quantum transport phenomena in 3D TI such as, Shubnikov de Hass (SdH) oscillations, weak antilocalization (WAL), universal conductance fluctuation (UCF), and Aharonov–Bohm effects have been already observed in nanowires, nanoribbons and thin films [9–17]. Detecting the surface states by charge transport is more challenging due to unavoidable bulk conductance. Therefore, in order to sort out the surface contribution, the bulk electrical conductance has to be eliminated or considerably suppressed. That is possible by reducing the thickness of the samples. The experimental data on charge transport of ultra thin samples related to the contribution of the surface states can be very informative in understanding the properties of TIs. So far, most of experimental results on 3D TI which came from Bi₂Se₃, Bi₂Te₃ compounds and Sb₂Te₃ have received little attention. This may have result from the fact that bulk Sb₂Te₃ is heavy *p*-type concentrated compound. However, the recent study of Sb₂Te₃ thin films by means of tunneling microscopy revealed well separated linear energy dispersion of surface states as a 2D massless Dirac fermions system [18]. The results indicate on possibility to observe fingerprint of the surface states by charge transport measurement. In this paper we report on fabrication of perfect single crystalline Sb₂Te₃ nanoflakes and study their magneto-transport properties. Especially, obtained oscillations on magnetoresistance (MR) allow us to reveal spin polarized nature of the surface states.

* Corresponding author at.: Institute for Physical Research, NASRA, Ashtarak 0203, Armenia.
E-mail address: sergeyhar56@gmail.com (S.R. Harutyunyan).
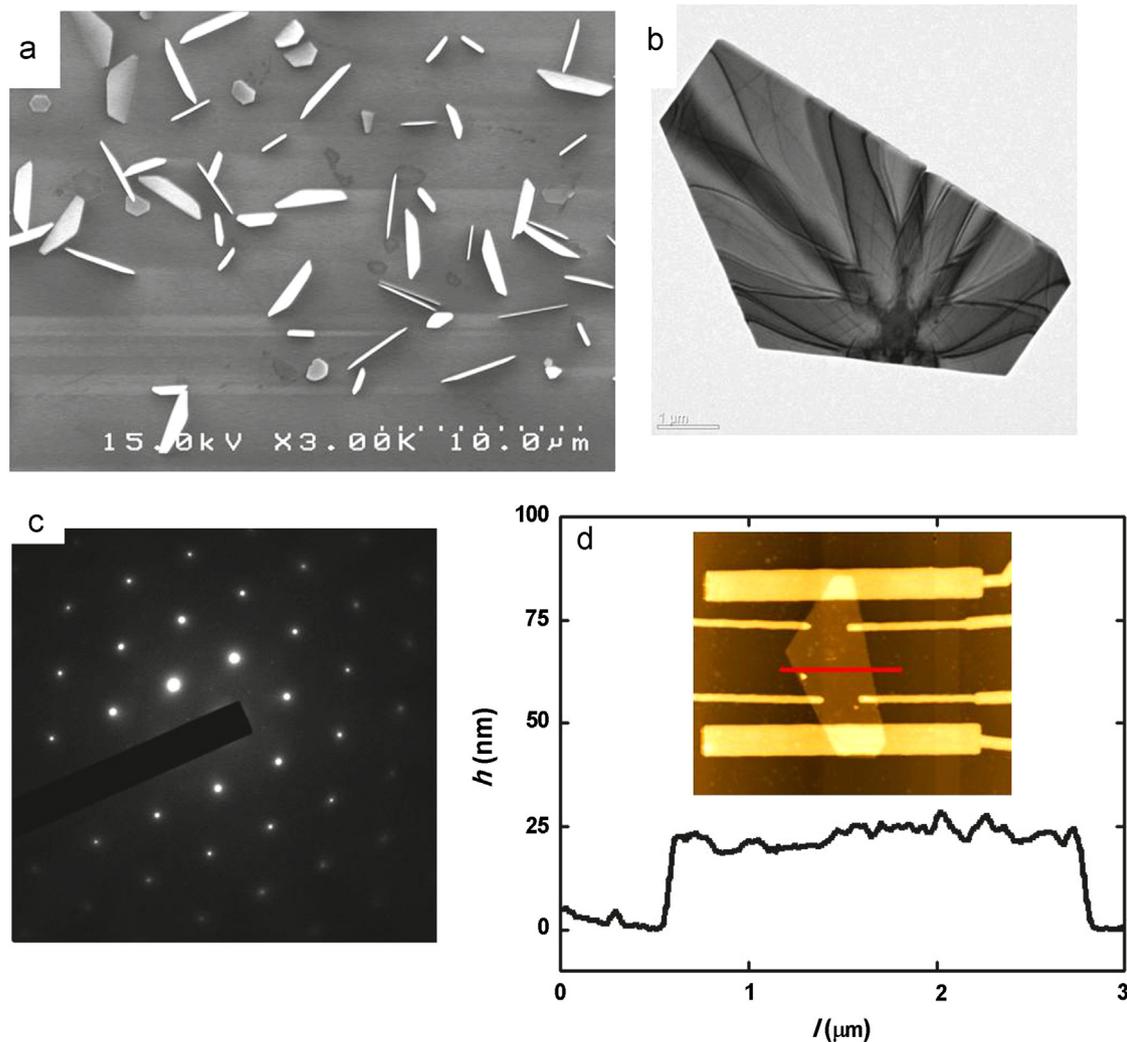
Fig. 1. (a) The grown nanoflakes. (b) TEM image of a single nanoflake. (c) TEM diffraction pattern of the nanoflake. (d) AFM topography with the height profile across the 25 nm thick patterned nanoflake.

2. Sample preparation and characterization

Single crystalline Sb_2Te_3 nanoflakes (hexagonal c axis is perpendicular to the flat surface) of various thicknesses were grown by a vapor phase deposition method on SiO_2/Si substrate using as a source material the polycrystalline Sb_2Te_3 [19,20]. The growth chamber represents itself a quartz glass tube which has been evacuated to a pressure 10^{-6} Torr. The polycrystalline Sb_2Te_3 was located at the end of the tube. The substrate has been placed horizontally along the tube next to the source material. The end of the tube containing the source was heated to 550 °C and resulting temperature gradient along the tube provided mass transfer to the substrate. Dimensions and shapes of the obtained nanoflakes varied over the length of the substrate and depend on local temperature of the substrate. A part of the substrate with accumulated nanoflakes is shown in Fig. 1a. Some of the free standing nanoflakes of suitable thickness were transferred by means of a micromanipulator to the standard 16 terminal chip for further patterning and measurement. A transmission electron microscope (TEM) diffraction pattern and the image of one of the grown nanoflakes are presented in Fig. 1b,c, and confirm that samples are single crystals. The free standing nanoflake with dimensions $l=5$ μm, $d=25$ nm (average width $w=2$ μm) was selected for measurements, where l is the length and d is the thickness of the nanoflake. The Sb/Te atomic ratio defined by means of Energy Dispersive X-ray Spectroscope corresponds to $(41 \pm 1)/(59 \pm 1)$. The leading wires of

Au/Ni were fabricated using electron beam lithography. The sample selected for the measurements had symmetrically positioned Hall contacts. An atomic force microscope (AFM) image of the patterned samples with leading wires is shown in Fig. 1d.

Transport measurements were carried out by a four-probe method (the width of the current and voltage probes were ~300 nm and 50 nm respectively) in a physical properties measurement system (PPMS) with magnetic fields up to 9 T at 2 K and 300 K. The magnetoresistance was defined as $(100\%) \times (R_B{-}R_0)/R_0$, where $R_B{=}R(B)$ is the resistance in magnetic field and R_0 is the resistance without magnetic field. The probe current (2 μA) was directed in crystallographic ab plane and MR was investigated for transverse directions of the magnetic field induction vector $\boldsymbol{B}$. The Hall voltage was taken as half the difference between two opposite directions of the induction vector $\boldsymbol{B}$.

3. Results and discussion

The temperature dependence of the longitudinal resistance R_{xx} of the nanoflake is shown in Fig. 2a and has metallic behavior. The magnetic-field dependence of the transverse resistance R_{xy}, shown in the same figure, is practically linear throughout the range of measurement and exhibits p-type conduction. The obtained hole concentration $n=1/(R_{xy} \times e)$ and mobility $\mu=R_{xy} \times d/(B \times \rho)$ are
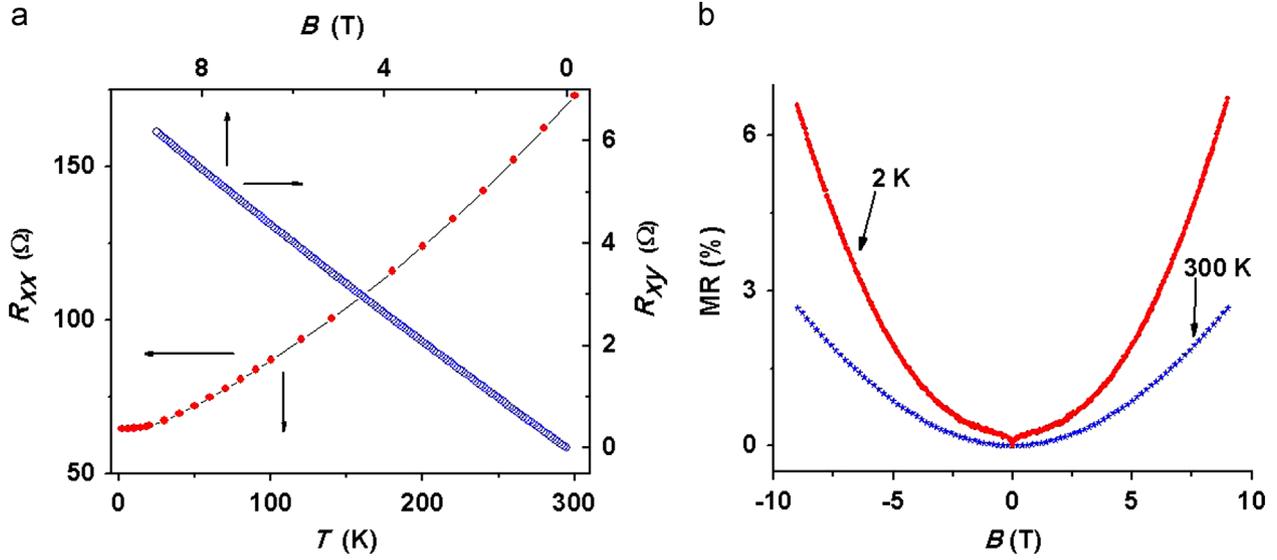
a

b

Fig. 2. (a) Temperature dependence of the longitudinal resistance R_{xx} and field dependence of the transverse resistance R_{xy}. (b) Magnetoresistance of the nanoflake at 2 K and 300 K.

$n = 3 \times 10^{26} \, \text{m}^{-3}$, $\mu = 0.0145 \, \text{m}^2/\text{V s}$ at 2 K and $n = 2 \times 10^{26} \, \text{m}^{-3}$, $\mu = 0.0075 \, \text{m}^2/\text{V s}$ at 300 K, where ρ is the resistivity of the nanoflake and e is an elementary charge. The concentration of holes in the nanoflake exceeds the concentrations typically observed in the bulk Sb_2Te_3. The increased carrier density implies an increase in the number of intrinsic defects, i.e. Sb vacancies and Sb_{Te} antisite defects (responsible for the hole generation), and therefore the number of defects is probably depends on the size of the sample [21]. This reflects the fact that reducing the size of the sample leads to an increase in the concentration of holes due to increasing the relative contribution from the surface of the nanoflake heavily occupied by defects. The magnetoresistance of the nanoflake in the region of ± 9 T is shown in Fig. 2b and the magnitude strongly depends on the temperature of the sample. The ordinary positive MR effect is caused by deflection of charge carriers under the Lorentz force. According to Kohler's rule $R(B)/R(B=0) \approx 1 + (\mu \times B)^2$ and the obtained MR curves reflect existing considerable difference in mobility of charge carriers at different temperatures.

The MR curve of the nanoflake exhibits the zero-field anomaly at 2 K. The anomaly presumably is the consequence of the WAL effect [15]. The amplitude of the anomaly is approximately 0.1 Ω at 2 K. The effect is inherent property of topological insulators and indicates the response of the surface states to magnetic field.

In case of strong spin-orbit coupling, when the momentum is strongly coupled with spin and protected by time reversal symmetry, the backscattering is forbidden. The activation of magnetic field causes the breaking of the symmetry (allowing the back-scattering) that results in abrupt increase of the resistance. Note that the WAL effect clearly seen at low temperature gradually smeared with temperature (Fig. 3) due to a decrease of the phase coherence length at higher temperature and is not observed at 300 K. In order to identify the surface states through WAL effect it is convenient to fit the magnetoconductance $\Delta G_{xx} = G_{xx}(B) - G(0)_{xx}$ by the Hikami–Larkin–Nagaoka (HLN) equation in the strong spin-orbit coupling limit [22]:

$$\Delta G_{WAL} = G(B) - G(0) = \alpha \frac{e^2}{2\pi^2 \hbar} \left[\Psi\left(\frac{1}{2} + \frac{B_\varphi}{B}\right) - \ln\left(\frac{B_\varphi}{B}\right) \right] \quad (1)$$

where α is WAL coefficient, $\Psi(x)$ is the digamma function, $B_\varphi = \hbar/4eL_\varphi^2$ and L_φ is the phase coherence length which characterizes the mesoscopic electron interference. Applying Eq. (1) to the experimental curves, the fitting parameters of α and B_φ were obtained.
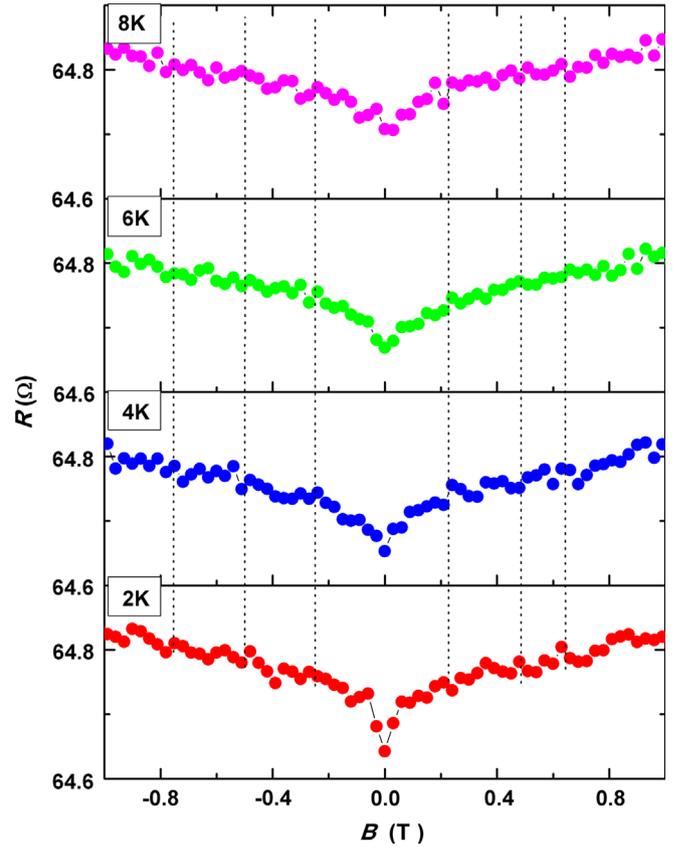

Fig. 3. WAL anomaly and UCF features at different temperatures; the vertical dot lines mark the same features at different temperatures.

The value of α should be 1, 0, and -0.5 for orthogonal, unitary and symplectic cases, respectively. Topological surface states, should belong to the symplectic case and therefore the value of α should be equal to -0.5 for one surface state and -1 for a thin film with top and bottom surface states [23]. Fig. 4 shows fit of Eq. (1) to the experimental data. The value of α derived from the fit curves is -0.71 and L_φ varied from ~ 300 nm to ~ 100 nm as temperature changed from 2 K to 8 K. Note that in previous works

on Sb_2Te_3 nanowire and thin film the following values of $\alpha=-0.42$ and $\alpha=-1$ correspondingly were obtained [16,17]. The monotonous reduction of L_φ with increasing T has also been observed for other TI systems. A power law fit of L_φ with T, presented in Fig. 5, gives $L_\varphi \sim T^{-0.49}$ which agrees well with the theoretical value for 2D systems [24]. However, we cannot confirm with the certainty that observed WAL effect comes from the topologically protected surface states of the nanoflake. The obtained value of $\alpha=-0.71$ indicates that the surface states may be partially mixed with the bulk states as a consequence of the large concentration of the holes in the nanoflake, and the bulk states in presence of strong spin-orbit coupling also can present quasi-2D WAL behavior. As shown in Fig. 3, the resistance fluctuates as the magnetic field changes resembling universal conduction oscillations. UCF curve consists of the aperiodic features that are observed repeatedly i.e. the similar features are observed in the different $R(B)$ curves measured at the different temperatures (Fig. 3). The fluctuations are strongly temperature-dependent. UCF are sample specific fluctuations in conductance of

mesoscopic samples that occur as function of magnetic field, chemical potential or impurity configuration and was observed in many mesoscopic TIs. UCF arises from the interference between all possible paths electron can take in traversing the sample. A smooth background was subtracted from the initial $R(B)$ dependence to analyze the UCF. The root mean square of the conductance fluctuations $\delta G_{rms}=(<[\delta G(B)-<\delta G(B)>]^2>)^{1/2}$, where $<\ldots>$ stands for the ensemble average, decays from nearly 0.044 to 0.034 e^2/h when the temperature increases from 2 to 6 K, implying that the oscillations are not of the thermal noise origin. It is known that the UCF amplitude undergoes the average reduction when the sample dimensions are longer than L_φ, which holds in our case. The 2D UCF theory predicts $\delta G_{rms}=0.86(e^2/h)/(2N)^{1/2}$ at $T=0$ K and equals to ~ 0.06 e^2/h for the geometry of our sample, which agrees well to the experimental value in orders, here $N=(L \times w)/L_\varphi^2$ represents the number of independent phase-coherent regions on the TI's surface [25,26]. However, we assume that the obtained fluctuations are not only of UCF origin, but they have mixed with SdH oscillations. These SdH oscillations have the form of beats and their amplitudes are comparable with the amplitude of UCF. The same fine structure exists in the $R_{xy}(B)$ dependence.

Fig. 5a and b shows the second derivative of $R_{xy}(B)$ and $R_{xx}(B)$ with respect to B, where the nod appears nearly at the same field for both dependences. The beating effect implies that the existing SdH oscillations have two closely spaced frequency components and comparable amplitudes. Such kind of oscillations previously observed on 2D electron gas (2DEG) systems where SdH oscillations were created with different (spin-up and spin-down) spin-polarized subbands of electrons [27–29]. Recently, a Rashba spin splitting of a two-dimensional electron gas was demonstrated in the topological insulator Bi_2Se_3 by angle-resolved photoemission spectroscopy [30]. This spin splitting means that, instead of one degenerate electron gas, there are two electron gases with a slightly different electron density separated in energy by $\Delta E=2\delta k_F$, where δ is Rashba parameter [31]. When the applied magnetic field increases, the Landau energy levels move to the Fermi level E_F, and the conduction occurs when each sublevel (spin-up and spin-down) crosses E_F, providing a modulated oscillation. Thus, the beating pattern arises from the existence of two kinds of carriers, and the sum of their concentrations at Fermi level. The nodes of the oscillations occur in the region of magnetic field in which there
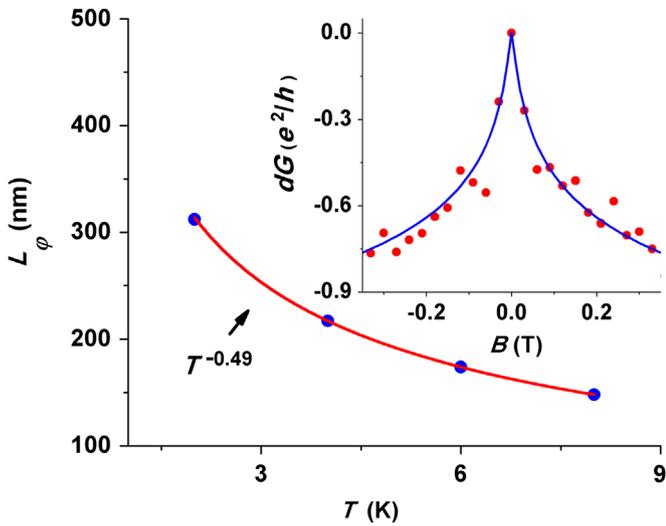

Fig. 4. Temperature dependence of the phase coherence length with power law fit. The inset shows the conductance near zero fields at 2 K with the fit by the HLN equation.
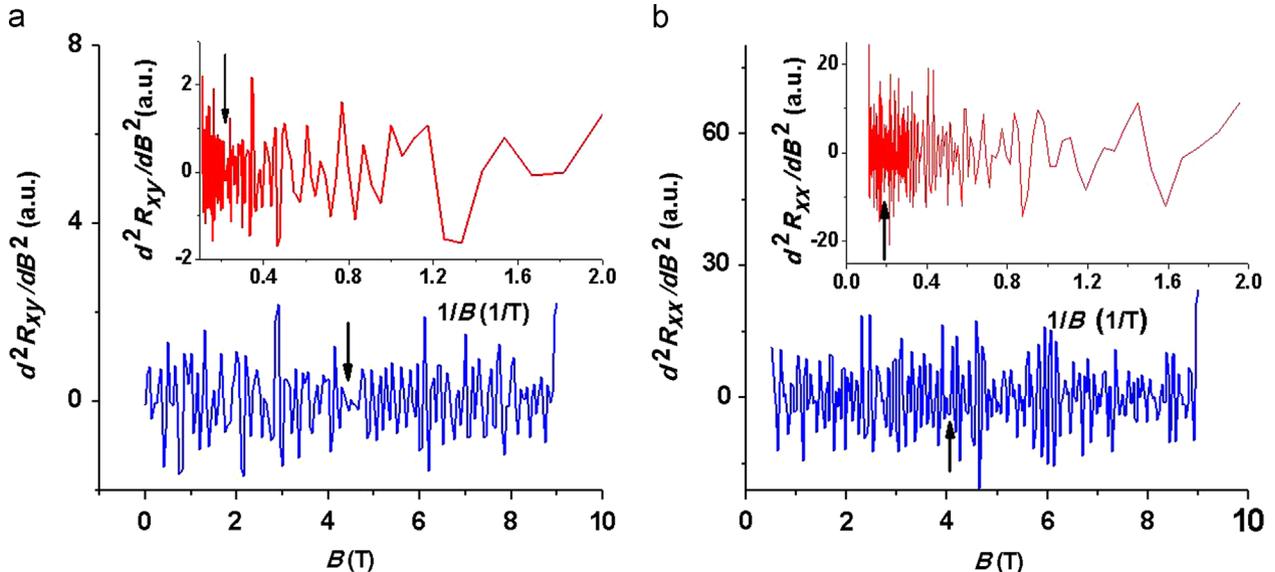

Fig. 5. (a, b) The oscillations of $R_{xy}(B)$ and $R_{xx}(B)$ resistances against B and $1/B$ (in the insets).The arrows indicate the nods the position of which coincides on both $R_{xy}(B)$ and $R_{xx}(B)$ curves.
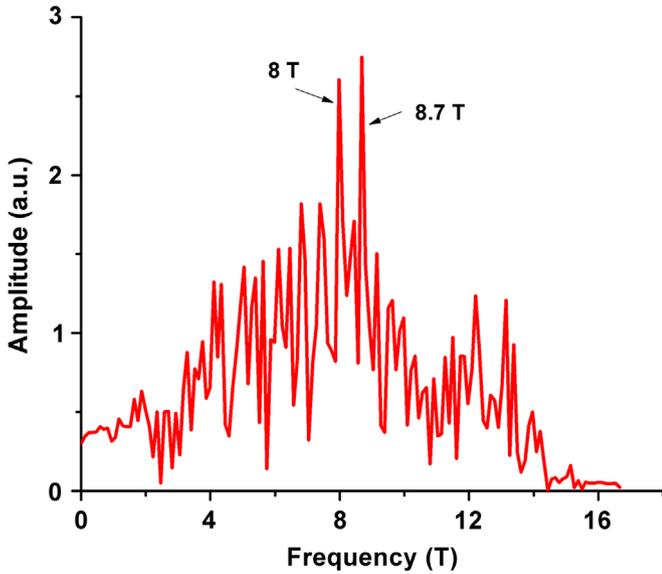
Fig. 6. FFT spectrum of the $R_{xx}(1/B)$ oscillations.

is no coincidence of energy levels at Fermi level. Application of Fast Fourier Transform (FFT) to the $R(1/B)$ oscillations has allowed us to reveal the spectrum with two well defined frequencies that we ascribe to the states with spin-up and spin-down polarizations (Fig. 6).

The noisy background in the FFT spectrum and the deviation from pure $1/B$ periodicity are presumably due to the contribution of UCF onto the clear SdH oscillations. Then, taking into account the density of states of a 2DEG at zero magnetic field, $D(E)=m^*/2\pi h^2$ for each electron spin system, the Rashba parameter can be deduced from the expression $\delta = \Delta n/2 \times D(E) \times k_F$, where $k_F = (2\pi N_S)^{1/2}$ wave vector of surface electrons, N_S is total number of the surface electrons, $\Delta n = N_1 - N_2$ is the difference in number of surface carrier at zero field between both possible spin orientations $N_1 = F_1 \times e/h$, $N_2 = F_2 \times e/h$, F_i is frequency of SdH oscillations for each spin orientation. The effective mass m^* of the upper and lower valence bands in Sb_2Te_3 is anisotropic and varies from $0.034m_e$ to $1.24m_e$ [32]. In our estimations we used the value of $0.034\ m_e$. The obtained Rashba parameter is equal to $\delta = 0.75 \times 10^{-11}$ eV m, whereas the energy gap between the two spin polarized subbands is $\Delta E = 2\delta k_F = 2.4$ meV. The obtained values of δ and ΔE are comparable with that observed previously in the semiconductor 2DEGs.

4. Conclusion

In the present work, the single crystal Sb_2Te_3 nanoflake with the thickness of 25 nm has been synthesized via the vapor phase deposition growth method. The mobility and number of carriers are obtained through the Hall resistance measurement data. The obtained magnetoresistance shows pronounced WAL effect. Using the 2D localization theory α of -0.71 and L_φ of ~ 300 nm are obtained at 2 K. The phase coherence length L_φ depends on temperature with a relation $L_\varphi \sim T^{-0.49}$ confirming the 2D nature of the WAL in this Sb_2Te_3 nanoflake. The observed fluctuations in the magnetoresistance attributed to the result of the combined contribution of UCF and SdH oscillations of the 2DEG. FFT spectrum of the obtained SdH oscillations reveals two well defined frequencies that we ascribe to the states with spin-up and spin-down polarizations. The obtained Rashba parameter and an energy gap between the two spin polarized subbands are $\delta = 0.75 \times 10^{-11}$ eV m and $\Delta E = 2.4$ meV correspondingly. We

disposed to ascribe the obtained oscillations to the topologically protected surface states, realizing at the same time that there are not enough evidences in our measurements. Additional experiments will be needed to carry out, especially the thickness-dependent and angle-dependent magnetoresistance measurements, which will be the task of our future work.

References

[1] C. Wood, Rep. Prog. Phys. 51 (1988) 459.
[2] B.Y.u. Yavorsky, N.F. Hinsche, I. Mertig, P. Zahn, Phys. Rev. B 84 (2011) 165208.
[3] V.A. Kulbachinskii, A. Yu., R.A. Kaminsky, K. Lunin, Y. Kindo, K. Narumi, S. Suga, M. Kawasaki, N. Sasaki, P. Miyajima, Lostak, P. Hajek, Semicond. Sci. Technol. 17 (2002) 1133.
[4] H. Zhang, Ch-H. Liu, X.-L. Qi, X. Dai, Zh. Fang, Sh-Ch. Zhang, Nat. Phys. 5 (2009) 438.
[5] J. Zhang, C.-Z. Chang, Z. Zhang, J. Wen, X. Feng, K. Li, M. Liu, K. He, L. Wang, X. Chen, Q.-K. Xue, X. Ma, Y. Wang, Nat. Commun. 2 (2011) 574.
[6] M.Z. Hasan, C.L. Kane, Rev. Modern Phys. 82 (2011) 3045.
[7] J.E. Moore, Nature 464 (2010) 194.
[8] Yoichi Ando, S.-C. Zhang, Physics 1 (2008) 6.
[9] J.G. Analitis, R.D. McDonald, S.C. Riggs, J.H. Chu, G.S. Boebinger, I.R. Fisher, Nat. Phys. 6 (2011) 960.
[10] H. Steinberg, D.R. Gardner, Y.S. Lee, P. Jarillo-Herrero, Nano Lett. 10 (2010) 5032.
[11] J. Lee, J. Park, J.-H. Lee, J.S. Kim, H.-J. Lee, Phys. Rev. B 86 (2012) 245321.
[12] S.S. Hong, J.J. Cha, D. Kong, Y. Cui, Nat. Commun. 3 (2012) 756.
[13] S. Matsuo, T. Koyama, K. Shimamura, T. Arakawa, Y. Nashihara, D. Chiba, K. Koboyashi, T. Ono, C.-Z. Chang, K. He, X.-C. Ma, Q.-K. Xue, Phys. Rev. B 85 (2012) 075440.
[14] L. Bao, L. He, N. Meyer, X. Kou, P. Zhang, Z.-G. Chen, A.V. Fedorov, J. Zou, T.M. Riedemann, T.A. Lograsso, K.L. Wang, G. Tuttle, F. Xiu, Nat. Commun. 2 (2012) 726.
[15] J.H. Bardarson, J.E. Moore., Rep. Prog. Phys. 76 (2013) 056501.
[16] Johannes Gooth Bacel Hamdou, August Dorn, Eckhard Pippel, Kornelius Nielsch, Appl. Phys. Lett. 102 (2013) 223110.
[17] Y. Takagaki, A. Giussani, K. Perumal, R. Calarco, K.-J. Friedland., Phys. Rev. B. 86 (2012) 125137.
[18] Y. Jiang, Y. Wang, M. Chen, Z. Li, C. Song, K. He, L. Wang, X. Chen, X. Ma, Q.-K. Xue, Phys. Rev. Lett. 108 (2012) 016401.
[19] Y. Takagaki, B. Jenichen, U. Jahn, M. Ramsteiner, K.-J. Friedland, J. Lahnemann, Semicond. Sci. Technol. 26 (2011) 125009.
[20] Hui Li, Jie Cao, Wenshan Zheng, Yulin Chen, Di Wu, Wenhui Dang, Kai Wang, Hailin Peng, Liu Zhongfan, J. Am. Chem. Soc. 134 (2012) 6132.
[21] Y.S. Kim, M. Brahlek, N. Bansal, E. Edrey, G.A. Kapilevich, K. Iida, M. Tanimura, Y. Horibe, S.-W. Cheong, S. Oh, Phys. Rev. B 84 (2011) 073109.
[22] S. Hikami, A.I. Larkin, Y. Nagaoka, Prog. Theor. Phys. 63 (1980) 707.
[23] H.-T. He, G. Wang, T. Zhang, I.-K. Sou, G.K.L. Wong, J.-N. Wang, H.-Z. Lu, S.-Q. Shen, F.-C. Zhang, Phys. Rev. Lett. 106 (2011) 166805.
[24] B.L. Altshuler, A.G. Aronov, D.E. Khmelnitsky, J. Phys. C: Solid State Phys. 15 (1982) 7367.
[25] P.A. Lee, A.D. Stone, H. Fukuyama, Phys. Rev. B 35 (1987) 1039.
[26] Zhaoguo Li, Taishi Chen, Haiyang Pan, Fengqi Song, Baigeng Wang, Junhao Han, Yuyuan Qin, Xuefeng Wang, Rong Zhang, Jianguo Wan, Dingyu Xing, Guanghou Wang, Sci. Rep. 2 (2012) 595.
[27] B. Das, D.C. Miller, S. Datta, R. Reifenberger, W.P. Hong, P.K. Bhattacharya, J. Singh, M. Jaffe., Phys. Rev. B 39 (1989) 1411.
[28] Ikai Lo, J.K. Tsai, W.J. Yao, P.C. Ho, Li-Wei Tu, T.C. Chang, S. Elhamri, W. C. Mitchel, K.Y. Hsieh, J.H. Huang, H.L. Huang, Wen-Chung Tsai, Phys. Rev. B 65 (2002) 161306.
[29] M.A. Hidalgo, R. Cangas, Phys. E: Low-dimens. Syst. Nanostruct. 42 (2010) 1329.
[30] P.D.C. King, R.C. Hatch, M. Bianchi, R. Ovsyannikov, C. Lupulescu, G. Landolt, B. Slomski, J.H. Dil, D. Guan, J.L. Mi, E.D.L. Rienks, J. Fink, A. Lindblad, S. Svensson, S. Bao, G. Balakrishnan, B.B. Iversen, J. Osterwalder, W. Eberhardt, F. Baumberger, P.h. Hofmann, Phys. Rev. Lett. 107 (2011) 096802.
[31] Y.u.A. Bychkov, E.I. Rashba, J. Phys. C: Solid State Phys. 17 (1984) 6039.
[32] O. Madelung, Semiconductors: Data Handbook, 3rd ed., Springer, Berlin, 2004.